Relaxor-ferroelectric crossover in $(Bi_{1/2}K_{1/2})TiO_3$: Origin of the spontaneous phase transition and the effect of an applied external field

Manabu Hagiwara,[1,*] Yoshitaka Ehara,[2] Nikola Novak,[2] Neamul H. Khansur,[3] Azatuhi Ayrikyan,[3] Kyle G. Webber,[3] and Shinobu Fujihara[1]

[1]*Department of Applied Chemistry, Faculty of Science and Technology, Keio University, 3-14-1 Hiyoshi, Kohoku-ku, Yokohama 223-8522, Japan*

[2]*Institute of Materials Science, Technische Universität Darmstadt, 64287 Darmstadt, Germany*

[3]*Department of Materials Science and Engineering, Friedrich-Alexander-Universität Erlangen-Nürnberg, 91058 Erlangen, Germany*

The temperature evolution of polar order in an A-site complex perovskite $(Bi_{1/2}K_{1/2})TiO_3$ (BKT) has been investigated by measurements of dielectric permittivity, depolarization current, and stress-stain curves at elevated temperatures. Upon cooling from high temperatures, BKT first enters a relaxor state and then spontaneously transforms into a ferroelectric state. The analyses of temperature and frequency dependence of permittivity have revealed that polar nanoregions of the relaxor phase appear at temperatures higher than 560 °C, and also that their freezing at 296 °C triggers the spontaneous relaxor-ferroelectric transition. We discuss the key factors determining the development of long-range polar order in A-site complex perovskites through a comparison with the relaxor $(Bi_{1/2}Na_{1/2})TiO_3$. We also show that application of biasing electric fields and compressive stresses to BKT favors its ferroelectric phase, resulting in a significant shift of the relaxor-ferroelectric transition temperature towards higher temperatures. Based on the obtained results, electric field-temperature and stress-temperature phase diagrams are firstly determined for BKT.

I. INTRODUCTION

Development of long-range polar order in perovskite ferroelectric oxides (with the general formula ABO_3) is a key factor determining their dielectric, ferroelectric, and electromechanical properties. In classical ferroelectrics such as $BaTiO_3$ (BT) and $PbTiO_3$ (PT) the long-range order is formed upon cooling below Curie temperature (T_C) by the dipole-dipole interaction, and thereby a macroscopic ferroelectric domain structure appears. The formed ferroelectric domain structure and its nonlinear relationship with the electric field significantly contribute to the dielectric and piezoelectric responses of the classical ferroelectrics [1,2]. In perovskites having multiple cations with different sizes, valences, or polarizabilities at a crystallographically equivalent site [e.g., $Pb(Mg_{1/3}Nb_{2/3})O_3$ (PMN)] or in those having lattice defects induced by a chemical substitution [e.g., $(Pb_{1-3x/2}La_x)(Zr_yTi_{1-y})O_3$ (PLZT)], the formation of long-range polar order is prohibited by the random fields and random bonds [3]. Hence, the so-called short-range ordered relaxor (R) state is formed, which is characterized by a broad temperature dependence of dielectric permittivity with a frequency-dependent dielectric maximum temperature (T_m) [4,5]. Relaxor-based solid solutions are used in a wide variety of piezoelectric applications owing to their excellent electromechanical properties [6,7].

Characteristic behavior of canonical relaxors can be explained by assuming the existence of polar nanoregions (PNRs) [4,5]. At temperatures above the Burns temperature (T_B) [8], relaxors exist in a nonpolar paraelectric (PE) state without any polar order. Upon cooling below this critical temperature, PNRs grow with decreasing temperature. In the high-temperature range, PNR dynamics are thermally excited and the spatial and temporal averages are the same. Relaxors within this temperature range are called ergodic relaxors (ERs) [5]. With further decreasing of the temperature, the dynamics of PNRs slows down and the longest relaxation time in the system diverges at the freezing temperature (T_f) [9,10]. The state below T_f is referred to as nonergodic relaxor (NR) [5]. An application of a sufficiently large electric field to relaxors below T_f can irreversibly transform them into a ferroelectric (FE) state with macroscopic domains, leading to a considerable decrease in dielectric permittivity and loss tangent as well as in their frequency dispersion [11]. Upon heating above T_f, the field-induced ferroelectric state transforms back into the ergodic relaxor state. In nonconventional relaxors, where relaxor and ferroelectric states are competitive at zero field, the transition from a relaxor state to a ferroelectric state occurs spontaneously, i.e., without applying an external field. B-site complex relaxors $Pb(Sc_{1/2}Nb_{1/2})O_3$ (PSN) and $Pb(Sc_{1/2}Ta_{1/2})O_3$ (PST) are known to exhibit such a spontaneous phase transition between ferroelectric and relaxor states [12–14]. It has been discovered that the evolution of the polar order in PST and PSN are strongly affected by some factors including cationic ordering and lattice defects. The degree of order of the B-site cations in PSN and PST can be controlled through long-time thermal annealing at a relatively low temperature around 1000 °C [12,13]. The single-crystal PST with ordered B-site cations undergoes the spontaneous R-FE transition, whereas that with disordered B-site cations exhibits the normal relaxor behavior [12]. A high concentration of A-site (Pb^{2+}) vacancy in PST and PSN stabilizes the relaxor state to eliminate the spontaneous transition into the ferroelectric state [13,14]. Solid-solution relaxors such as PMN-PT and PLZT are also reported to show the spontaneous R-FE transition in a limited composition range [15–17].

---
*hagiwara@applc.keio.ac.jp

Due to the increasing concern about the toxicity of Pb, Bi-based A-site complex perovskites $((Bi_{1/2}A'_{1/2})TiO_3$, where A' is a monovalent cation such as Na^+, K^+, or Ag^+) have been extensively studied as alternatives for the Pb-based ferroelectrics [18–20]. Among them, $(Bi_{1/2}Na_{1/2})TiO_3$ (BNT) is the most studied material due to its strong ferroelectricity and ability to form solid solutions exhibiting enhanced piezoelectric properties at the morphotropic phase boundary compositions [21,22]. BNT has disordered Bi^{3+} and Na^+ ions in the A site and undergoes crystallographic phase transitions from cubic to tetragonal at $540\,^\circ C$ and from tetragonal to rhombohedral at $263\,^\circ C$ [23]. The dielectric permittivity of BNT below the tetragonal-rhombohedral transition temperature shows a relaxorlike strong frequency dispersion at room temperature [19,24], which has been attributed to the dielectric response of the rhombohedral PNRs embedded in the nonpolar tetragonal matrix [25]. It has been reported that the application of an electric field to BNT results in a large irreversible volume change, showing an electric-field-induced R-FE transition analogous to other Pb-based relaxors [26]. More detailed studies on the field-induced R-FE transition have been reported for BNT-based solid-solution relaxors, such as $(Bi_{1/2}Na_{1/2})TiO_3$-xBaTiO$_3$ (BNT-xBT) and $(Bi_{1/2}Na_{1/2})TiO_3$-$x(Bi_{1/2}K_{1/2})TiO_3$ (BNT-xBKT) systems. For these solid solutions, the stability regions of relaxors and field-induced FE states were determined by means of electric field (E)-temperature (T) phase diagrams [27,28]. Moreover, recent studies have shown that application of uniaxial compressive stress (σ) also affects the polar order of the BNT-based solid solutions in a similar way to the electric field. Hence, σ-T phase diagrams have been proposed [29,30]. Such E-T and σ-T phase diagrams are not only scientifically important but also helpful for the practical development of BNT-based lead-free piezoelectric ceramics because the transition between ferroelectric and relaxor states has been shown to predominantly determine their depolarization temperature and the electric-field-induced strain response [31,32].

In contrast to BNT-based compositions, there have been fewer reports on the properties and R-FE transition behavior of $(Bi_{1/2}K_{1/2})TiO_3$ (BKT), which is a structural analog of BNT having disordered Bi^{3+} and K^+ ions at the A site. BKT displays tetragonal symmetry at room temperature [18] and shows multiple crystallographic phase transitions from tetragonal to pseudocubic at $260\,^\circ C$ and pseudocubic to cubic at $380\,^\circ C$ [33]. Investigations of BKT by transmission electron microscopy have found that laminar macroscopic ferroelectric domains, similar to those of BT, exist in individual grains, which with increasing temperature gradually disappear between $280\,^\circ C$ and $450\,^\circ C$ [34]. Hiruma *et al.* have reported that high-quality BKT ceramics show both normal ferroelectriclike clear polarization hysteresis and relaxorlike broad temperature dependence of dielectric permittivity [35]. Recently, we have found that BKT is a relaxor at elevated temperatures and spontaneously transforms into a low-temperature FE state around $300\,^\circ C$ [36,37], which is far different from the behavior of BNT. BKT is the only example so far of an A-site complex perovskite exhibiting the spontaneous R-FE transition and should thus be a good model material for studying the role of the A-site ions on the development of long-range ferroelectric polar order. However, the mechanism and origin

of such a spontaneous R-FE transition in BKT have not been investigated yet. When we compare the above-described A-site complex perovskites BNT and BKT, the following fundamental question arises: Why is the long-range ferroelectric order spontaneously developed only in BKT? To address this question, we investigated the temperature-dependent dielectric, strain, and polarization behavior of polycrystalline BKT samples. A key factor affecting the evolution of the polar order in BKT is suggested. We also show the effect of biasing electric and compressive stress fields on the R-FE transition. Lastly, based on results of these measurements, E-T and σ-T phase diagrams for BKT are proposed.

II. EXPERIMENTAL PROCEDURE

Polycrystalline BKT ceramic samples with two different shapes, thin pellets and thick cylinders, were prepared to perform electrical and mechanical measurements at varying temperatures, respectively. To reveal the properties of BKT, preparation of ceramic samples with large grains is important because the ferroelectric and piezoelectric properties of BKT are degraded in fine-grained ceramics with grain sizes less than $1\,\mu m$ [37,38]. Because of the low melting point of BKT (at $1070\,^\circ C$ [39]), prolonged sintering (typically over 20 h) at temperatures near the melting point is needed to obtain course-grained ceramic samples. However, the evaporation of Bi and K during such prolonged sintering can cause formations of secondary phases [39,40]. For this reason, special attention should be paid to the processing of BKT ceramics to obtain stoichiometric samples with a large grain size ($>1\,\mu m$). We prepared pellet and cylindrical samples using BKT powders synthesized by hydrothermal and conventional solid-state reactions, respectively.

The hydrothermal BKT powder was synthesized using anatase TiO$_2$ (99.9%, Toho Titanium Co., Ltd.) and Bi(OH)$_3$ (99.9%, Kojundo Chemical Laboratory Co., Ltd) as Ti and Bi sources, respectively. The details of the procedure have been described elsewhere [41]. In brief, a 12-M KOH aqueous solution dispersing a stoichiometric ratio of TiO$_2$ and Bi(OH)$_3$ was heated to $160\,^\circ C$ and immediately cooled to $110\,^\circ C$ and held for 6 h. The product was washed with ethanol and dried at $60\,^\circ C$ overnight. The resulting hydrothermal BKT powder was uniaxially pressed and subsequently cold isostatically pressed at 350 MPa into pellets. The green bodies were embedded in sacrificial BKT powder prepared by the below-described solid-state reaction to prevent the evaporation of Bi and K during sintering and then sintered at $1060\,^\circ C$ for 100 h to achieve a sufficient grain growth. After sintering, the samples were ground and polished to a final dimension of 0.7 mm in thickness and 7.0 mm in diameter. Platinum electrodes with a diameter of 5.5 mm were then sputtered on the polished faces of the samples.

The hydrothermal BKT powder described above has a superior sinterability and a good chemical stability against the prolonged sintering, thereby providing pellet samples with a high electrical insulation resistance [41]. However, the hydrothermal powder contains a significant number of hydroxyl groups as a lattice defect [42]. We found that thicker cylindrical samples could not be obtained from this powder because a strong volume expansion of the samples

occurred during the long-time sintering process due to the elimination of the lattice hydroxyl groups as H$_2$O vapor. Similar volume expansion during sintering has been reported for hydrothermal BT powders [43]. Therefore, cylindrical samples were prepared using another BKT powder synthesized by a solid-state reaction. Anatase TiO$_2$, KHCO$_3$ (99.5%, Wako Pure Chemical Industries), and Bi$_2$O$_3$ (99.9%, Kojundo Chemical Laboratory Co., Ltd), were weighted according to the stoichiometric formula and ball-milled using ethanol and yttrium-stabilized zirconia balls for 24 h. The powder mixture was then dried and calcined in an alumina crucible at 750 °C for 10 h. A second calcination step at 850 °C for 10 h with an intermediate milling cycle was performed to achieve better homogeneity of the final powder. The resulting powder was ball-milled again for 24 h, then pressed and sintered in the same condition as the hydrothermal powder. After the sintering, the cylindrical sample with a height of 6 mm and a diameter of 5.8 mm were ground from the sintered body. Before the measurements described below, the sample was annealed at 400 °C for 30 min and cooled to room temperature with the rate of 1 °C/min to remove internal stresses induced by machining and to ensure that the samples were depolarized.

The real and imaginary parts of the relative permittivity of the pellet sample were measured at frequencies between 100 Hz and 1 MHz in a box furnace with a custom-made sample holder and an impedance analyzer (HP 4192A, Hewlett-Packard Co.) with a heating/cooling rate of 2 °C/min. Temperature-dependent dielectric response to a dc bias voltage signal superposed by a small 1-V signal excitation voltage at a frequency of 1 kHz was measured. Constant dc fields up to 7.5 kV/cm were applied using a high-voltage source (high-voltage supply/amplifier/controller, Trek Model 610E, Trek, Inc). For depolarization current measurement, the pellet sample was poled in silicone oil at 90 °C under a dc electric field of 80 kV/cm for 10 min and field-cooled to room temperature. The depolarization current during heating was measured using a source meter (model 2400, Keithley) at a heating rate of 2 °C/min up to 400 °C. The remanent polarization P_r was calculated as a function of temperature according to the following equation:

$$P(T) = \frac{1}{a} \int \frac{I(T)}{A} dT, \qquad (1)$$

where a, I, and A are the heating rate, the measured depolarization current, and the electrode area, respectively.

In this work, mechanical uniaxial stress-strain behavior as well as dielectric permittivity under a constant stress were measured as a function of temperature. These measurements were conducted in a 30-kN screw-type load frame (Zwick, Z030) equipped with a differential loading dilatometer and split furnace. A detailed description of the experimental setup is given elsewhere [44]. During the stress-strain measurement, the cylindrical sample was uniaxially loaded to −500 MPa with a loading rate of 5 MPa/s, followed by unloading with the same rate. For the measurement of temperature dependence of dielectric permittivity under a mechanical stress, the sample was heated at 2 °C/min under a constant stress between −0.8 and −400 MPa and its capacitance was measured parallel to the loading direction at a frequency of 1 kHz using an impedance analyzer (HP 4192A, Hewlett-Packard Co.).
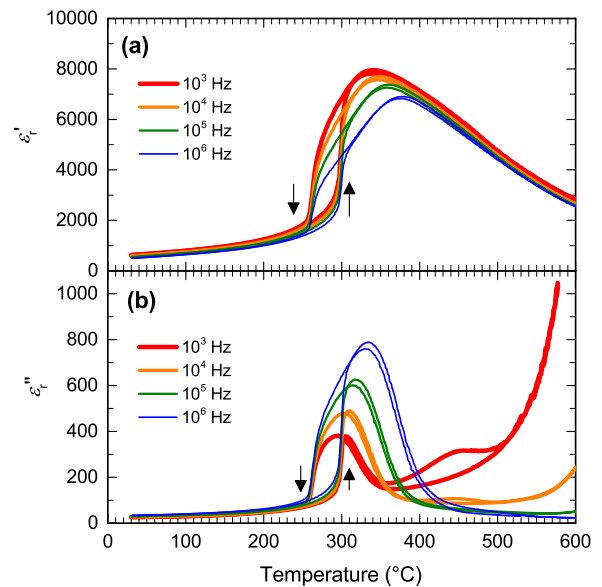

FIG. 1. Temperature dependence of (a) real part ε' and (b) imaginary part ε'' of dielectric permittivity of BKT measured at varying frequencies from 10^3 to 10^6 Hz.

III. RESULTS AND DISCUSSION

X-ray diffraction (XRD) measurements confirmed that both the pellet and cylindrical samples were the single phase of the tetragonal BKT. Any superlattice diffraction peaks were not observed in the XRD patterns for these samples (not shown here) as reported elsewhere [37], indicating that Bi^{3+} and K$^+$ ions in the BKT samples were completely disordered. The grain size of the pellet sample sintered for 100 h was approximately 1.0 μm. The cylindrical sample sintered for 20 h had a smaller grain size of approximately 0.6 μm, and thus the electrical and mechanical properties may be affected by the grain size effect [36,37]. The weight losses for the pellet and cylindrical samples during sintering were 1% and 2%, respectively, showing that these samples contain only a small amount of A-site (Bi^{3+} or K$^+$) vacancies.

Figure 1 depicts the temperature dependence of the real (ε_r') and imaginary (ε_r'') parts of relative dielectric permittivity for polycrystalline BKT. As previously reported, the sample shows a dielectric anomaly with a strong thermal hysteresis around 300 °C, which has been attributed to the spontaneous transition between the high-temperature relaxor state and the low-temperature ferroelectric state [36]. Temperatures of the R → FE and FE → R transitions are denoted as T_{R-FE} and T_{FE-R}, respectively, which were determined from the peak of the temperature derivative of permittivity ($d\varepsilon_r'/dT$) in the cooling and heating runs, respectively. Dielectric behavior of BKT closely resembles that reported for PST and PSN, although the T_{R-FE} and T_{FE-R} of BKT are much higher (T_{R-FE} = −2.2 °C and 94.8 °C for PST and PSN ceramics, respectively [13,14]).

As a first step towards understanding the evolution of polar ordering in BKT, we attempted to determine T_B, at which the PNRs appear, from the analysis of the dielectric behavior of the relaxor state. Viehland et $al.$ have been demonstrated that the temperature dependence of dielectric permittivity of
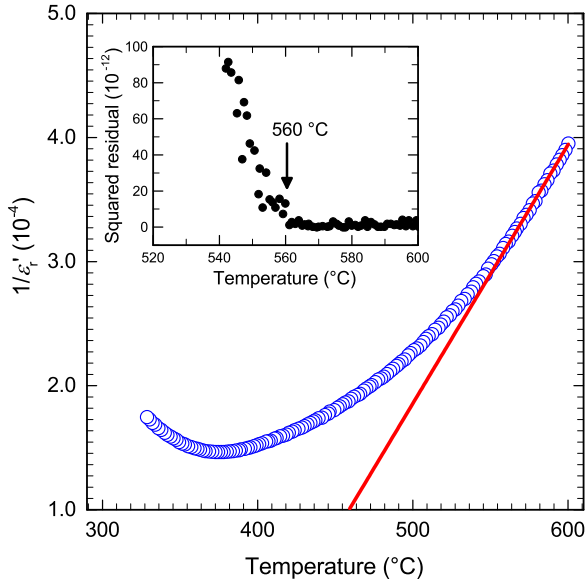
FIG. 2. Inverse of dielectric permittivity as a function of temperature at 10^6 Hz for the relaxor state of BKT. Solid line is the fittings to the C-W law [Eq. (2)]. The inset shows the squared residual of the fitting to the C-W law as a function of temperature. The arrow in the inset presents the temperature for the onset of deviation from the C-W low.

the canonical relaxor PMN deviates from the following well-known Curie-Weiss (C-W) law below T_B due to short-range correlations between PNRs [45]:

$$\varepsilon'_r = \varepsilon_c + \frac{C}{T - T_{CW}}, \qquad (2)$$

where ε_c is a constant including temperature-independent contributions to permittivity, T_{CW} is the Curie-Weiss temperature, and C is the Curie constant. Such a deviation from the C-W law in relaxors has been applied to many other compositions, such as PLZT [17], PSN [46,47], and Ba(Ti$_{1-x}$Sn$_x$)O$_3$ [48], to determine their T_B. Figure 2 shows the C-W plot for BKT, made from the data given in Fig. 1. The solid line represents the fitting to the C-W law [Eq. (2)] using 22 data points measured at temperatures between 580 °C and 600 °C. It is obvious that the dielectric data of BKT notably deviate from the C-W law with decreasing temperature. The squared residual between the measured data and the C-W fitting [$(1/\varepsilon_{meas} - 1/\varepsilon_{calc})^2$, where ε_{meas} and ε_{calc} are the measured and calculated relative permittivity, respectively] is plotted as a function of temperature in the inset of Fig. 2. Although the fitting was performed using the data at the temperatures between 580 °C and 600 °C, the residual remains almost zero within a wider temperature range. The onset of the deviation was found at 560 °C, approximately 180 °C higher than T_m at 1 MHz. This observation is similar to PLZT whose T_B is 170 °C above T_m [4]. However, due to the small fitting area, there still remains a possibility that PNRs appears at higher temperatures. Vögler *et al.* recently conducted the measurement of temperature-dependent Young's modulus on BNT-xBT ($x = 0.03, 0.06,$ and 0.12) and suggested that PNRs are formed in a broad temperature range starting around ~720 °C [49], which is much higher than the previously reported T_B of 421 °C (for

$x = 0.03$) determined by the dielectric measurement [50]. Nevertheless, our dielectric measurement demonstrates that PNRs in BKT exist at temperatures below 560 °C.

It is interesting to note that the determined temperature for the onset of the deviation from the C-W law is very close to T_C of the potassium-containing bismuth-layer-structured ferroelectric K$_{0.5}$Bi$_{4.5}$Ti$_4$O$_{15}$ ($T_C = 555$ °C [51]), in which the ferroelectricity arises from the Bi-rich pseudoperovskite (K$_{0.5}$Bi$_{2.5}$Ti$_4$O$_{13}$)$^{2-}$ layers. This fact might relate to the formation mechanism of PNRs in BKT. A very recent pair distribution function analysis with a combination of a reverse Monte Carlo simulation has revealed that Bi^{3+} and K$^+$ ions in BKT are highly disordered and form small regions with Bi-rich and K-rich local compositions [52]. From these observations, it is reasonable to consider that the Bi-rich region in BKT, which should have a high T_C, acts as a core to form PNRs. Kreisel *et al.* have suggested a similar structural model for BNT where polar clusters of Bi^{3+}TiO$_3$ and Na$^+$TiO$_3$ are embedded in an antiferroelectric matrix [53].

PNRs formed at elevated temperatures grow with decreasing temperature and their dynamics slows down; then some of them freeze at T_f. Below T_f, relaxors exist in the nonergodic relaxor state. It is widely accepted that the macroscopic dielectric response of relaxors during the freezing process is described by the following Vogel-Fulcher (V-F) relationship [9,10,54,55]:

$$\omega = \omega_0 \exp\left[-\frac{E_a}{k_B(T_m - T_f)}\right], \qquad (3)$$

where k_B is Boltzmann's constant, E_a is the activation energy, ω is the measurement frequency, and ω_0 is the Debye frequency. The relationship between inverse T_m and ω for BKT is shown in Fig. 3. Fitting was performed only for the data at frequencies higher than 650 Hz to avoid the influence of the dielectric loss, which becomes significant at low frequencies. Using Eq. (3), the fit parameters $T_f = 296 \pm 5$ °C,
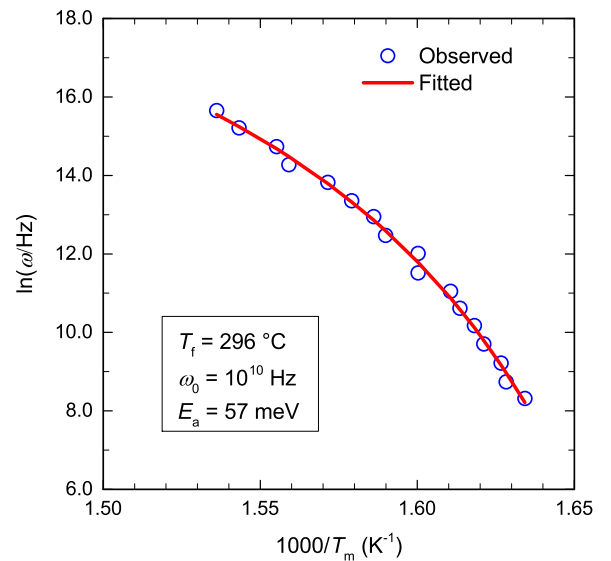

FIG. 3. Relationship between the inverse of the temperature of the dielectric maximum of BKT and the measurement frequency. The solid line is the fittings to the V-F law [Eq. (3)].

$E_a = 57 \pm 10$ meV, and $\omega_0 = 10^{10}$ Hz have been extracted. It is important that the determined T_f exists within the thermal hysteresis of a dielectric anomaly due to the first-order R-FE transition. This strongly suggests that the freezing of PNRs in the ergodic relaxor state triggers the spontaneous transformation into the ferroelectric state; i.e., there is no nonergodic relaxor state in BKT.

Ergodicity/nonergodicity in a relaxor is often evaluated by measuring the polarization response as a function of electric field, i.e., hysteresis loops. Normal ferroelectriclike rectangular hysteresis is observed when a high electric field is applied in the NR temperature range due to the irreversible transition into a ferroelectric state, whereas a pinched hysteresis is observed in the ER temperature range due to reversibility of the field-induced R-FE transition. However, pinched hysteresis could not be obtained in BKT due to the conductivity in the ER temperature range. Therefore, we attempted to confirm the ergodicity in BKT above T_{R-FE} from the measurement of stress-strain curves instead of the polarization hysteresis measurement. As reported for BNT-0.06BT relaxors [30], a uniaxial compressive stress can induce a long-range ferroelectric order similar to the application of electric field. Thus, the nonergodicity/ergodicity in a relaxor can be judged by the observation of macroscopic mechanical constitutive behavior, e.g., remanent strain (S_r). Figure 4 presents representative stress-strain curves measured for a cylindrical BKT sample at 25 °C, 100 °C, 200 °C, and 300 °C. At 300 °C, the sample is just above T_{R-FE}. At temperatures below T_{R-FE}, the stress-strain behavior is initially linear below a critical mechanical stress (~300 MPa for 25 °C). With an increasing stress there is the development of a nonlinear stress-strain response. Similar mechanical behavior has also been observed in other perovskite ferroelectrics, such as PZT [56], BT [57], and BiFeO$_3$-x(Bi$_{1/2}$K$_{1/2}$)TiO$_3$ [58], which is understood to be due to the nucleation and growth of ferroelastic domain walls. At these temperatures, the ferroelastic curves display a significant hysteresis and a large remanent strain. At elevated tempera-
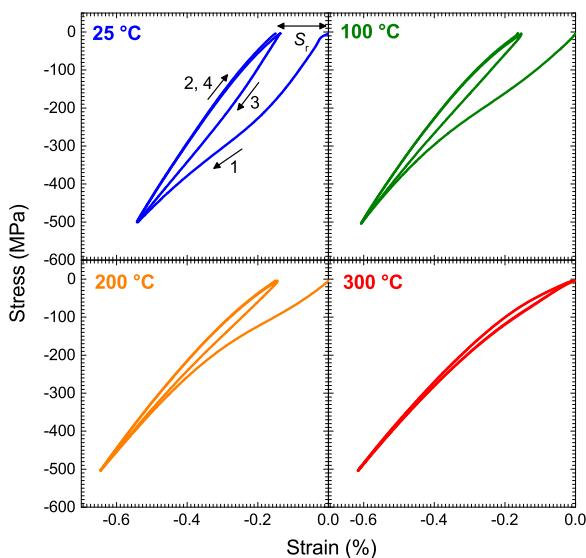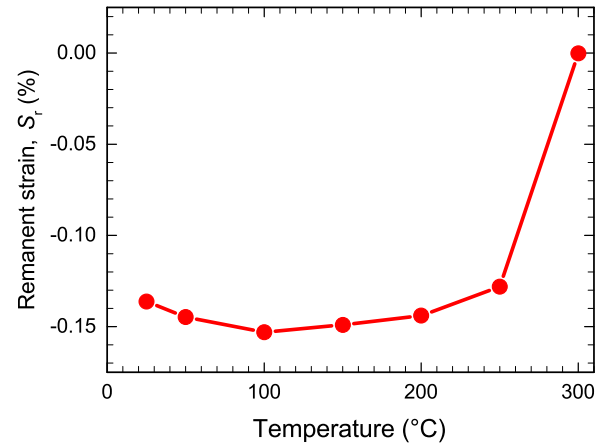

FIG. 5. Remanent strain of BKT as a function of temperature.

tures, however, there is a decrease in the hysteresis, where at 300 °C, the stress-strain curve shows a closed hysteresis loop without remanent strain. When we plot the observed remanent strain as a function of temperature (Fig. 5), it is evident that the remanent strain suddenly vanishes at T_{R-FE}, whereas it is almost constant at lower temperatures. These results are consistent with a FE → ER transition during heating. If BKT is in a nonergodic relaxor state above T_{R-FE}, a remanent strain during mechanical loading should be observed because of the stress-induced transition into a long-range ferroelectric order. The result shown here thus clearly demonstrates the absence of nonergodic relaxor state in BKT as indicated by the V-F analysis.

As further evidence for the absence of the nonergodic relaxor state above T_{R-FE} in BKT, we also examined the depolarization behavior during heating after electrical poling treatment. Figure 6 shows the temperature dependence of remanent polarization calculated from the depolarization current. It is observed that remanent polarization vanishes very sharply at T_{R-FE} in one step, showing that the depolarization of BKT is caused by the first-order FE → ER transition. Sharp depolarization behavior of BKT is in contrast with that of BNT and BNT-xBT, which exhibit multiple depolarization

FIG. 4. Stress-strain behavior of BKT measured at varying temperatures. Arrows indicate the loading direction.
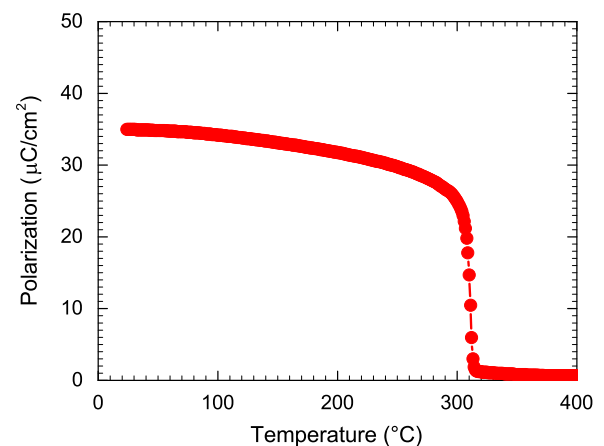

FIG. 6. Remanent polarization of BKT as a function of temperature.

steps due to complex electrical and crystallographic phase transitions [31,59,60]. Thus the depolarization behavior also confirms that no intermediate phase exists between ferroelectric and ergodic relaxor states in BKT and supports the result of V-F analysis that T_{R-FE} coincides with T_f. It should also be mentioned that the observed depolarization temperature of BKT is much higher than that of BNT, which depolarizes at $187\,°C$ [59], showing that BKT is suitable for piezoelectric applications requiring a high-temperature stability of the polarized state.

The above results revealed that the evolution of polar order in BKT is quite simple: PNRs appear at temperatures higher than $560\,°C$, and their freezing at $296\,°C$ triggers the spontaneous first-order phase transition into the ferroelectric state with the long-range polar order. It is known that BNT shows a relaxorlike behavior even at room temperature. Here we discuss the origin of such a difference between BKT and BNT. It is widely accepted that a relaxor state is induced by local random fields resulting from randomly distributed different cations or lattice defects. In complex perovskites, the random fields originate from the difference in ionic radius and in the valence of cations occupying a crystallographically equivalent site. Chu *et al.* [14], who studied the spontaneous R-FE transition in *B*-site complex perovskites, have suggested that the difference of polarizing power (eZ/R^2, where e is the electronic charge, Z is the valence, and R is the ionic radius) of the *B*-site cations determines whether the long-range polar order is developed in them or not. For example, PMN with a large polarizing power difference between Mg^{2+} and Nb^{5+} ions is a typical relaxor, whereas $Pb(Fe_{1/2}Nb_{1/2})O_3$ with a much smaller polarizing power difference belongs to normal ferroelectric. PSN and PST show the spontaneous R-FE transition because they have an intermediate polarizing power difference. In the present case of BKT and BNT, considering the ionic radii of *A*-site cations (Bi^{3+} : 120 pm [61], Na^+ : 139 pm [62], K^+ : 164 pm [62]), BKT should have a larger polarizing power difference than BNT. Thus the polarizing power difference does not provide a convincing explanation of the experimental fact that the long-range polar order is more prone to be formed in BKT rather than in BNT.

Another factor that may affect the development of polar order is the crystal system of the perovskite lattice, which is governed by the following Goldschmidt tolerance factor t:

$$t = \frac{R_A + R_o}{\sqrt{2}(R_B + R_o)}, \tag{4}$$

where R_A, R_B, and R_O are radii of *A*-site, *B*-site, and oxygen ions, respectively. Perovskites with t near unity tend to have a cubic or tetragonal symmetry, whereas those with $t < 1$ favor lower symmetries, such as orthorhombic and rhombohedral. Because t for BNT is 0.952, BNT is composed of PNRs with rhombohedral symmetry at room temperature [25]. With substituting larger K^+ for Na^+ (i.e., with increasing x in the BNT $- x$BKT system), the rhombohedral symmetry with antiphase octahedral tilting gradually changes to the tetragonal one with cation off-centering along the c axis [63]. As a result, the pure BKT with t value very close to unity (0.995) has a relatively large tetragonal distortion ($c/a \sim 1.02$) at room temperature. It can be reasonably expected that PNRs in the ergodic relaxor state of BKT should also have a tetragonal

symmetry because a transition from the tetragonal phase to another phase with a lower symmetry upon heating is forbidden. In fact, a selected area electron diffraction pattern for a BKT ceramic at $400\,°C$, i.e., in the ergodic relaxor state, has been reported to show slightly elongated [100] spots [34], indicating the crystal lattice has a small tetragonal distortion even at this temperature. We consider that the tetragonal symmetry of the PNRs in BKT should be one possible factor inducing the transition into a long-range ordered ferroelectric state at T_f. As discussed above, *A*-site cations in both BNT and BKT, and Bi^{3+} and Na^+/K^+, are randomly distributed and the difference of their ionic radius should be the source of random fields. According to the spherical random-bond-random-field model developed by Pirc and Blinc [3], the long-range ordered ferroelectric state appears in a system with nonzero random fields when the interaction between PNRs (random bonds) is strong and its statistical probability distribution is narrow. Because the number of allowed polar directions for the tetragonal symmetry is smaller, i.e., six $\langle 001 \rangle$ directions, than that for the rhombohedral symmetry, i.e., eight $\langle 111 \rangle$ directions, the probability distribution of the interaction between the tetragonal PNRs in BKT should be narrower. The volume of the PNR grows with decreasing temperature and sharply increases near T_f. At this temperature, the interaction between PNRs in BKT is considered to become sufficiently strong to induce the transition into the long-range ordered ferroelectric state. The importance of the tetragonal symmetry for the occurrence of the spontaneous R-FE transition has also been suggested for the PMN-PT solid-solution relaxors [16].

The effect of biasing external fields on the spontaneous R-FE transition of BKT has been investigated by means of the temperature dependence of dielectric permittivity under constant electric or stress field. Figure 7 shows the result for the pellet sample measured at temperatures around T_{R-FE} under biasing electric fields. Although the measured permittivity under the largest applied field of 7.5 kV/cm shows a somewhat irregular temperature variation caused by the degraded insulation resistance, it is evident that the application of an electric field significantly increases both T_{R-FE} and T_{FE-R}. It should be noted that the applied electric fields studied here are below the coercive field of BKT at room temperature (~ 50 kV/cm [37]). These results demonstrate that even such a relatively small electric field facilitates the development of long-range polar order, leading to the notable increase of the R-FE transition temperature. It is also observed in Fig. 7 that the thermal hysteresis of the R-FE transition becomes smaller with increasing the biasing electric field. Because the transition is first order without the biasing field, the spontaneous polarization of the ferroelectric state discontinuously vanishes at T_{FE-R} as previously shown in Fig. 6. The reduction of the thermal hysteresis means that the transition gradually becomes second-orderlike with increasing applied electric field. For the *B*-site complex perovskite PSN, the thermal hysteresis has been found to completely vanish at the biasing electric field of 5 kV/cm [47]. In the present case of BKT, the dielectric permittivity under the 7.5 kV/cm still shows a clear thermal hysteresis, possibly attributed to the smaller polarizability of the ergodic relaxor state of BKT compared to PSN.

The effect of the compressive stress on the temperature evolution of permittivity is presented in Fig. 8. Dielectric
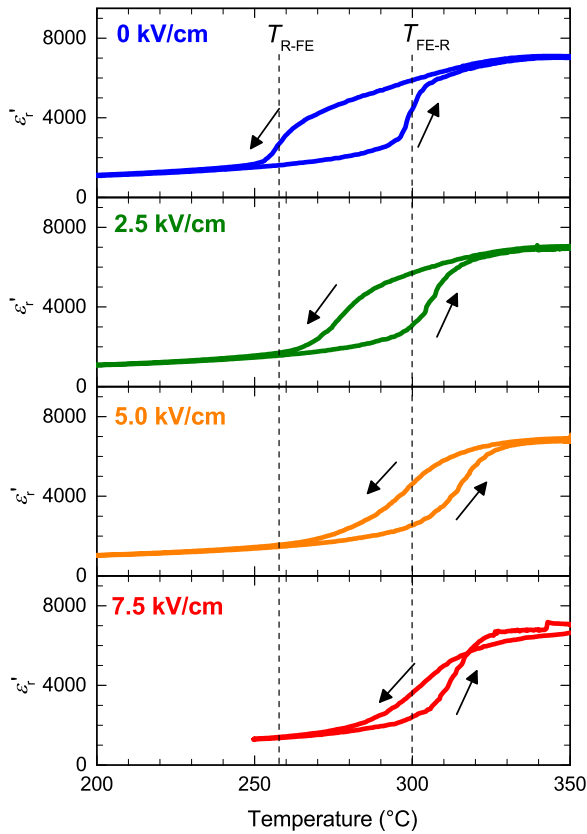
FIG. 7. Temperature dependence of dielectric permittivity of BKT measured at 10^6 Hz under the application of varying electric fields.

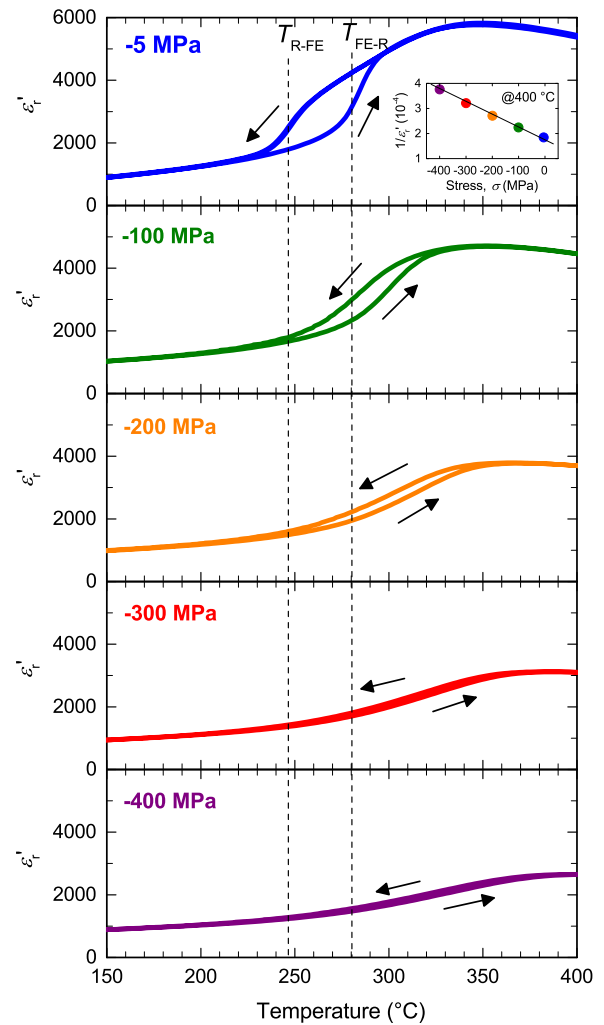FIG. 8. Temperature dependence of dielectric permittivity of BKT measured at 10^6 Hz under the application of varying stresses.

measurements under stress were performed on the cylindrical BKT sample. Compared with the pellet sample (Figs. 1 and 7), under the nearly stress-free condition (-5 MPa) the cylindrical sample exhibits slightly lower transition temperatures and also lower dielectric permittivity in the ergodic relaxor state. This is considered due to the smaller grain size in the cylindrical sample resulting from the shorter sintering time [37]. It is found that the application of stress produces two characteristic influences on the dielectric behavior of BKT: (i) a strong decrease in permittivity and (ii) broadening of the dielectric anomalies at T_{R-FE} and T_{FE-R}, both of which are not observed under the application of electric fields. The stress dependence of permittivity of a material often comes from the converse electrostrictive effect. Due to this effect, the permittivity of material is changed by an application of stress as follows [64]:

$$\frac{1}{\varepsilon_r'} = Q\varepsilon_0\sigma, \tag{5}$$

where ε_0 is the permittivity of vacuum and Q is the electrostrictive coefficient of the material, which is nearly independent of temperature [64]. As shown in the inset of Fig. 8, the observed compressive stress dependence of the permittivity of BKT at 400 °C well follows this relationship and the slope of the plot gives an electrostrictive coefficient $Q = 2.8 \times 10^{-2}$ m^4/C^2. This value is very close to that for the ordinary relaxor PMN (2.5×10^{-2} m^4/C^2 [64]). Thus the electrostrictive effect should be responsible for the strong

decrease in permittivity under the application of stress. On the other hand, the broadening of the transition is likely due to randomly oriented grains in the polycrystalline sample [65]. The differences of the crystallographic direction, size, and shape of each grain result in the different local stress field in individual grains. As a result, grains have a transition temperature slightly different from each other, leading to the broadened dielectric anomaly. The dielectric anomaly and the thermal hysteresis become unclear under the compressive stress because of the electrostrictive effect. Nevertheless, it is clear that the application of biasing stress also shifts the R-FE transition temperatures towards higher temperatures, similar to the electric field.

The phase relations of BKT determined by the measurements of permittivity, σ-S curves, and depolarization current are summarized as the E-T and σ-T phase diagrams in Fig. 9. As previously mentioned, the transition temperatures, T_{R-FE} and T_{FE-R}, were determined from the peak of the temperature derivative of permittivity. Thus, the phase diagrams proposed here should only be read in the temperature direction. At sufficiently high temperatures, BKT is in the paraelectric state without any polar order but has a compositional heterogeneity.
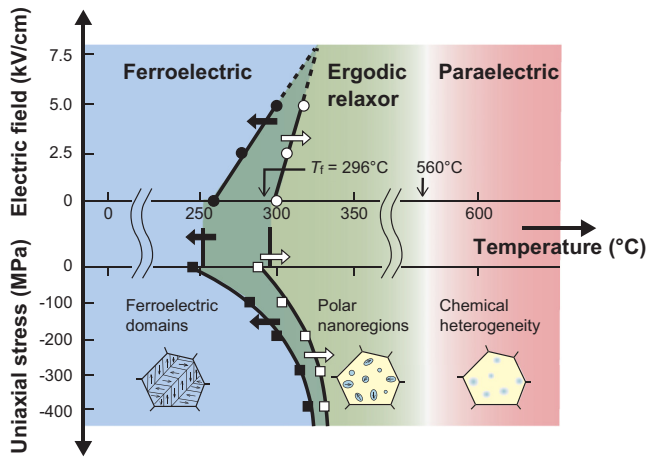
FIG. 9. E-T and σ-T phase diagrams for BKT. The microstructure models for the corresponding phases are also shown.

Upon zero-field cooling, PNRs appear around $560\,^\circ$C, grow in size with further decrease of temperature, and then freeze at $T_f = 296\,^\circ$C. The boundaries between paraelectric and ergodic relaxor states are shown using color gradation because of the possibility that the PNRs are formed at higher temperatures. The freezing of PNRs triggers the formation of long-range polar order, leading to the spontaneous phase transition in to the FE phase. The application of a biasing electric field induces polarization in the parallel direction to the field, whereas the application of stress induces polarization in plane perpendicular to direction of applied stress. Both of them favor the ferroelectric state, resulting in the significant shift of T_{R-FE} and T_{FE-R} towards higher temperatures. We have not studied T_B under biasing external electrical or mechanical fields. However, it has been reported for PSN that T_B is not influenced by the application of electric field [46], so it can be expected that $T_B(E)$ and $T_B(\sigma)$ lines in the phase diagrams may be nearly

vertical to the temperature axis. We believe that the observed high T_{FE-R} of BKT and its significant shift by external fields can motivate the development of BKT-based lead-free piezoelectric ceramics with high depolarization temperatures based on electric field/stress engineering, such as compositing with polar crystals such as ZnO [66,67].

IV. SUMMARY

In this study, we conducted the measurements of temperature dependences of dielectric permittivity, depolarization current, and stress-strain curves using high-quality BKT polycrystalline samples. PNRs in BKT are found to exist below $560\,^\circ$C by the observation of the deviation from the C-W law. Analysis of the V-F behavior of the relaxor state revealed that the spontaneous R-FE transition is triggered by the freezing of PNRs and also that there is no nonergodic state in BKT. Based on the comparison with the relaxor BNT, it is suggested that the tetragonal symmetry of BKT coming from the larger ionic radius of K^+ compared to Na^+ plays an important role in the development of long-range polar order. In addition, it was observed that the application of external electrical and mechanical fields facilitates the development of the long-range order, leading to the increase of both T_{R-FE} and T_{FE-R}. Lastly, we proposed E-T and σ-T phase diagrams for BKT dividing the regions of paraelectric, ergodic relaxor, and ferroelectric states.

[1] T. Tsurumi, J. Li, T. Hoshina, H. Kakemoto, M. Nakada, and J. Akedo, Appl. Phys. Lett. **91**, 182905 (2013).

[2] A. Pramanick, D. Damjanovic, J. E. Daniels, J. C. Nino, and J. L. Jones, J. Am. Ceram. Soc. **94**, 293 (2011).

[3] R. Pirc and R. Blinc, Phys. Rev. B **60**, 13470 (1999).

[4] G. A. Samara, J. Phys.: Condens. Matter. **15**, R367 (2003).

[5] A. A. Bokov and Z.-G. Ye, J. Mater. Sci. **41**, 31 (2006).

[6] S.-E. Park and T. R. Shrout, J. Appl. Phys. **82**, 1804 (1997).

[7] S. Zhang and F. Li, J. Appl. Phys. **111**, 031301 (2012).

[8] G. Burns and F. H. Dacol, Phys. Rev. B **28**, 2527 (1983).

[9] D. Viehland, S. J. Jang, L. E. Cross, and M. Wuttig, J. Appl. Phys. **68**, 2916 (1990).

[10] A. Levstik, Z. Kutnjak, C. Filipič, and R. Pirc, Phys. Rev. B **57**, 11204 (1998).

[11] M. L. Mulvihill, L. E. Cross, W. Cao, and K. Uchino, J. Am. Ceram. Soc. **80**, 1462 (1997).

[12] N. Setter and L. E. Cross, J. Appl. Phys. **51**, 4356 (1980).

[13] F. Chu, N. Setter, and A. K. Tagantsev, J. Appl. Phys. **74**, 5129 (1993).

[14] F. Chu, I. M. Reaney, and N. Setter, J. Appl. Phys. **77**, 1671 (1995).

[15] R. Jiménez, B. Jiménez, J. Carreaud, J. M. Kiat, B. Dkhil, J. Holc, M. Kosec, and M. Algueró, Phys. Rev. B **74**, 184106 (2006).

[16] H. Cao, J. Li, and D. Viehland, J. Appl. Phys. **100**, 034110 (2006).

[17] X. Dai, A. Digiovanni, and D. Viehland, J. Appl. Phys. **74**, 3399 (1993).

[18] C. F. Buhrer, J. Chem. Phys. **36**, 798 (1962).

[19] V. A. Isupov, Ferroelectrics **315**, 123 (2005).

[20] J.-H. Park, P. M. Woodward, J. B. Parise, R. J. Reeder, I. Lubomirsky, and O. Stafsudd, Chem. Mater. **11**, 177 (1999).

[21] T. Takenaka, K. Maruyama, and K. Sakata, Jpn. J. Appl. Phys. **30**, 2236 (1991).

[22] A. Sasaki, T. Chiba, Y. Mamiya, and E. Otsuki, Jpn. J. Appl. Phys. **38**, 5564 (1999).

[23] G. O. Jones and P. A. Thomas, Acta Crystallogr., Sect. B: Struct. Sci. **58**, 168 (2002).

[24] C.-S. Tu, I. G. Siny, and V. H. Schmidt, Phys. Rev. B **49**, 11550 (1994).

[25] S. B. Vakhrushev, V. A. Isupov, B. E. Kvyatkovsky, N. M. Okuneva, I. P. Pronin, G.A. Smolensky, and P. P. Syrnikov, Ferroelectrics **63**, 153 (1985).

[26] W. Jo and J. Rödel, Appl. Phys. Lett. **99**, 042901 (2011).

[27] E. Sapper, N. Novak, W. Jo, T. Granzow, and J. Rödel, J. Appl. Phys. **115**, 194104 (2014).

[28] Y. Ehara, N. Novak, S. Yasui, M. Itoh, and K. G. Webber, Appl. Phys. Lett. **107**, 262903 (2015).

[29] F. H. Schader, Z. Wang, M. Hinterstein, J. E. Daniels, and K. G. Webber, Phys. Rev. B **93**, 134111 (2016).

[30] Y. Ehara, N. Novak, A. Ayrikyan, P. T. Geiger, and K. G. Webber, J. Appl. Phys. **120**, 174103 (2016).

[31] E. Sapper, S. Schaab, W. Jo, T. Granzow, and J. Rödel, J. Appl. Phys. **111**, 014105 (2012).

[32] W. Jo, T. Granzow, E. Aulbach, J. Rödel, and D. Damjanovic, J. Appl. Phys. **105**, 094102 (2009).

[33] V. V Ivanova, A. G. Kapyshev, Y. N. Venevtsev, and G. S. Zhdanov, Izv. Akad. Nauk SSSR **26**, 354 (1962).

[34] M. Otoničar, S. D. Škapin, B. Jančar, R. Ubic, and D. Suvorov, J. Am. Ceram. Soc. **93**, 4168 (2010).

[35] Y. Hiruma, R. Aoyagi, H. Nagata, and T. Takenaka, Jpn. J. Appl. Phys. **44**, 5040 (2005).

[36] M. Hagiwara and S. Fujihara, Appl. Phys. Lett. **107**, 012903 (2015).

[37] M. Hagiwara and S. Fujihara, Jpn. J. Appl. Phys. **54**, 10ND10 (2015).

[38] Y. Hiruma, H. Nagata, and T. Takenaka, Jpn. J. Appl. Phys. **46**, 1081 (2007).

[39] J. König, M. Spreitzer, B. Jančar, D. Suvorov, Z. Samardžija, and A. Popovič, J. Eur. Ceram. Soc. **29**, 1695 (2009).

[40] J. König and D. Suvorov, J. Eur. Ceram. Soc. **35**, 2791 (2015).

[41] M. Hagiwara and S. Fujihara, J. Mater. Sci. **50**, 5970 (2015).

[42] M. Hagiwara, M. Ito, and S. Fujihara, J. Asian Ceram. Soc. **5**, 31 (2017).

[43] D. F. K. Hennings, C. Metzmacher, and B. S. Schreinemacher, J. Am. Ceram. Soc. **84**, 179 (2001).

[44] R. Dittmer, K. G. Webber, E. Aulbach, W. Jo, X. Tan, and J. Rödel, Acta Mater. **61**, 1350 (2013).

[45] D. Viehland, S. J. Jang, L. E. Cross, and M. Wuttig, Phys. Rev. B **46**, 8003 (1992).

[46] F. Chu, G. R. Fox, and N. Setter, J. Am. Ceram. Soc. **81**, 1577 (1998).

[47] E. L. Venturini, R. K. Grubbs, G. A. Samara, Y. Bing, and Z.-G. Ye, Phys. Rev. B **74**, 064108 (2006).

[48] C. Lei, A. A. Bokov, and Z.-G. Ye, J. Appl. Phys. **101**, 084105 (2007).

[49] M. Vögler, N. Novak, F. H. Schader, and J. Rödel, Phys. Rev. B **95**, 024104 (2017).

[50] J. Suchanicz and T. V. Kruzina, Mater. Sci. Eng. B **178**, 889 (2013).

[51] C.-M. Wang and J.-F. Wang, J. Am. Ceram. Soc. **91**, 918 (2008).

[52] B. Jiang, T. Grande, and M. Selbach, Chem. Mater. **29**, 4244 (2017).

[53] J. Kreisel, A. M. Glazer, P. Bouvier, and G. Lucazeau, Phys. Rev. B **63**, 174106 (2001).

[54] A. E. Glazounov and A. K. Tagantsev, Appl. Phys. Lett. **73**, 856 (1998).

[55] R. Pirc and R. Blinc, Phys. Rev. B **76**, 020101 (2007).

[56] A. B. Schäufele and K. H. Härdtl, J. Am. Ceram. Soc. **79**, 2637 (2005).

[57] G. Picht, K. G. Webber, Y. Zhang, H. Kungl, D. Damjanovic, and M. J. Hoffmann, J. Appl. Phys. **112**, 124101 (2012).

[58] E. T. Wefring, F. H. Schader, K. G. Webber, M.-A. Einarsrud, and T. Grande, J. Eur. Ceram. Soc. **36**, 497 (2016).

[59] Y. Hiruma, H. Nagata, and T. Takenaka, J. Appl. Phys. **105**, 084112 (2009).

[60] W. Jo, J. Daniels, D. Damjanovic, W. Kleemann, and J. Rödel, Appl. Phys. Lett. **102**, 192903 (2014).

[61] R. A. Armstrong and R. E. Newnham, Mater. Res. Bull. **7**, 1025 (1972).

[62] R. D. Shannon, Acta Crystallogr., Sect. A **32**, 751 (1976).

[63] I. Levin, I. M. Reaney, E.-M. Anton, W. Jo, J. Rödel, J. Pokorny, L. A. Schmitt, H.-J. Kleebe, M. Hinterstein, and J. L. Jones, Phys. Rev. B **87**, 024113 (2013).

[64] K. Uchino, S. Nomura, L. E. Cross, S. J. Jang, and R. E. Newnham, J. Appl. Phys. **51**, 1142 (1980).

[65] F. H. Schader, E. Aulbach, K. G. Webber, and G. A. Rossetti, J. Appl. Phys. **113**, 174103 (2013).

[66] J. Zhang, Z. Pan, P. X. Nie, Y.-S. Cui, B. Yang, J. Chen, and S-T. Zhang, Appl. Phys. Lett. **106**, 232904 (2015).

[67] Z. Pan, J. Chen, L. Fan, J. Zhang, S. Zhang, Y. Huang, L. Liu, L. Fang, and X. Xing, J. Am. Ceram. Soc. **98**, 3935 (2015).